

# Structural, magnetic and optical behavior of pristine and Yb doped CoWO<sub>4</sub> nanostructure

J. Juliet Josephine Joy · N. Victor Jaya

Received: 21 September 2012 / Accepted: 26 November 2012 / Published online: 18 December 2012  
© Springer Science+Business Media New York 2012

**Abstract** Nanocrystalline pure and Yb doped CoWO<sub>4</sub> nanostructures were synthesized successfully by single step chemical precipitation technique. The prepared sample was characterized by X-ray diffraction (XRD), Fourier transform infrared spectroscopy (FTIR) and thermal analysis (TGA). XRD pattern reveals the pure and doped CoWO<sub>4</sub> nanoparticles belongs to the monoclinic structure with the space group of P<sub>2/c</sub>. Electron microscopy studies clearly evidence the formation of round edged nanocubes with an average particle size of 60–80 nm, emerges in the polycrystalline nature. UV–Visible absorption spectra of Yb<sup>3+</sup> doped CoWO<sub>4</sub> nanocrystals shows a strong absorption peak at 278 nm due to CoWO<sub>4</sub> metal to ligand charge transfer within the [WO<sub>6</sub>]<sup>6-</sup> complex. Photoluminescence spectra of pure and doped CoWO<sub>4</sub> nanostructures substantiate the effect of Yb on the wolframite structure and its response for optical behavior. These results suggest that the addition of Yb into the Co-site on CoWO<sub>4</sub> has no significant contribution for luminescent enhancement when compared to pure one up to 5 % Yb concentration. Typical magnetization curve shows the mixed ferromagnetic and diamagnetic transition of CoWO<sub>4</sub> with respect to the Yb doping concentration.

## 1 Introduction

Inorganic metal oxide based phosphors plays a vital role in cathode-ray tubes, electroluminescent devices, plasma display panels and field emission displays [1]. Nanosize transition metal tungstates have received much attention owing

to their dominant luminescent behavior and their potential applications in various technologies. Some of the metal tungstates are more peculiar because of their electrical and magnetic behavior [2]. Among them CoWO<sub>4</sub> is most extensively studied material for photoluminescence, optoelectronics devices, scintillating material, microwave dielectrics and catalysis [3]. Generally, CoWO<sub>4</sub> belongs to the wolframite structure with monoclinic phase [4]. The rare-earth doped nanophosphors attain the optimum requirement of real life optical displays in their bulk form. Only limited investigations were reported in early research on rare earth doped transition metal tungstates [5]. We believe that the excellent chemical stability and luminescent nature of CoWO<sub>4</sub> nanostructure with suitable rare earth element will make it as a potential candidate for practical application.

Recent research on CoWO<sub>4</sub> mainly focuses on their nanostructural morphology such as nanorods, nanobelt, nanowires and nanoplates etc. [5]. Various methods are followed to synthesis cobalt tungstates with desired morphology. Most of the reported synthetic methods are solid state reaction, sol–gel, chemical precipitation, and hydrothermal process [5, 6]. The most inventive and simple way to synthesis the doped metal tungstates is chemical-precipitation method. The conventional ceramic method consumes long time, energy and uncontrolled particle growth. There is possibility to synthesize nanomaterials with desired morphology and size using hydrothermal and solvothermal methods. However, specific requirement of solvents and reaction vessel limits their wide applications. As a consequence to control the particle growth and morphology the above wet chemical synthesis method was much appreciated for nanoparticle synthesis. Of all the available trivalent rare-earth (RE) ions, Er<sup>3+</sup> and Yb<sup>3+</sup> are the most popular and effective ions for optical pumping. To the best of our knowledge there are no reports published elsewhere on

J. Juliet Josephine Joy · N. Victor Jaya (✉)  
Department of Physics, Anna University, Chennai 600025, India  
e-mail: victor@annauniv.edu

luminescent effect and magnetic behavior of wolframite  $\text{CoWO}_4$  with trivalent  $\text{Yb}^{3+}$  ion doping. In addition to the host material, foreign impurities also play a key role for obtaining the efficient luminescence [7].

In this present investigation for the first time we are reporting the magnetic, optical and luminescent behavior of Yb doped  $\text{CoWO}_4$  nanostructures. With respect to the doping concentration, the optical activity of the material was investigated by UV–Vis spectroscopy. Due to the trivalent  $\text{Yb}^{3+}$  ion, the room temperature mixed weak ferromagnetic and paramagnetic phase of the host material changed towards diamagnetic. The characteristic luminescence of the monoclinic  $\text{CoWO}_4$  wolframite was discussed with ambient temperature photoluminescence spectra.

## 2 Experimental techniques

Pure and  $\text{Yb}^{3+}$  doped  $\text{CoWO}_4$  wolframite were synthesized via single step chemical precipitation technique. Typical synthetic procedures were discussed [8] briefly; analytical grade cobalt II acetate (Alfa Aaser), yttrium III nitrate (Alfa Aaser) of various concentrations (1, 3 and 5 %) and disodium tungstate (Merck), dissolved in double distilled water separately under constant stirring. As prepared Cobalt metal-ion solution was added dropwise to tungstate solution over 15 min, the violet colored precipitates were formed. Immediately, 0.1 M of polyethylene glycol (PEG-mw 1000) was added to the above mixture as a surfactant. The stirring was continued until the complete precipitation followed by 15 h aging. Finally, the end product was separated by centrifugation and washed thoroughly with deionized water, ethanol and acetone consecutively. After drying at ambient temperature for 24 h, the powder was calcined at 600 °C for 6 h. For synthesis of a pure  $\text{CoWO}_4$  nanostructure, the same procedure was followed without  $\text{Yb}^{3+}$  cation solution as mentioned above.

XRD pattern of the wolframite nanostructure was taken from the BRUKER D5 Phaser, FTIR spectra of the samples were obtained from the Perkin FTIR spectrophotometer over range of 400–4,000  $\text{cm}^{-1}$ , UV–Vis spectrophotometer (Shimadzu UV-2450) was used to see the optical absorbance of the sample. For microstructure and morphological features high resolution scanning electron microscope (HRSEM) (HITACHI (Japan) SU6600-15 kV) and transmission electron microscope (TEM) (HITACHI (Japan) H-7650-80 kV) were directly used with Energy Dispersive Spectroscopy attachment. Magnetic studies of the prepared samples were carried out on Vibrating Sample Magnetometer (Lakshore VSM 7410), Thermal stability of the  $\text{CoWO}_4$  was studied using Thermo gravimetric Analyzer (TGA) (BRUKER SDT Q600 V8.0), and X-ray fluorescence spectrometer (PL) (S4 PIONEER BRUKER) was

used to analyze the luminescent characteristic of the material.

## 3 Results and discussion

### 3.1 Thermal analysis

Crystallization temperature of  $\text{CoWO}_4$  nanostructure during thermal decomposition was studied using Thermo gravimetric analysis. The typical curve of temperature versus mass change of the pure and  $\text{Yb}^{3+}$  doped  $\text{CoWO}_4$  are shown in Fig. 1. The observed weight loss in the TGA curve below the 200 °C is associated to the solvent evaporation. The major mass change in the range of 200–400 °C is mainly attributed to the precursor decomposition and evaporation of organic moieties. In addition to the above, very small and gradual weight loss between the temperatures 400–600 °C, ascribes the crystallization process which was confirmed by the plateau region observed in the TGA curve beyond the 600 °C. When compared to the pure, it was observed that Yb doped  $\text{CoWO}_4$  showed less crystallization temperature. This may be due to the strong interaction of trivalent  $\text{Yb}^{3+}$  ion in  $\text{Co}^{2+}$  lattice site. In order to control the grain growth and maintain the nanostructure of the sample, we have fixed the calcination temperature of 600 °C for our wolframite  $\text{CoWO}_4$ . Further, it has the good agreement with earlier reports [8, 9].

### 3.2 Phase analysis

Powder XRD pattern of chemically precipitated pure and Yb doped  $\text{CoWO}_4$  calcined at 600 °C are shown in Fig. 2. It clearly indicates the formation of single phase monoclinic

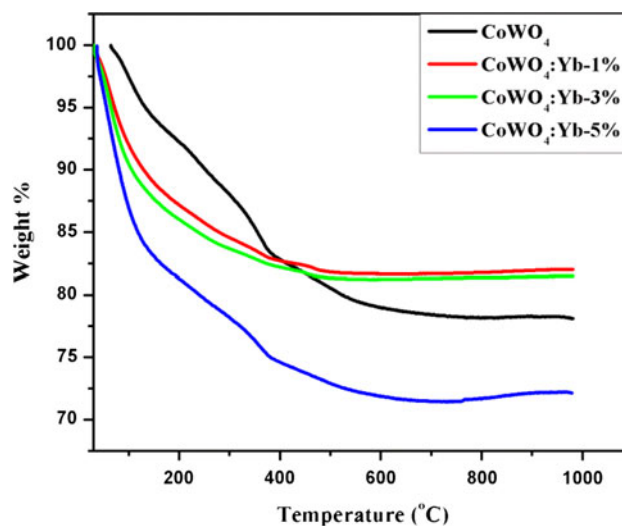


Fig. 1 TGA curve of as prepared pure and Yb doped  $\text{CoWO}_4$

CoWO<sub>4</sub> nanostructure with the space group of P<sub>2</sub>/c (13). Further it reveals that there is no ternary oxide phase due to WO<sub>4</sub> and Co<sub>3</sub>O<sub>4</sub>. All the peak position and their relative intensity were indexed with standard spectrum of [JCPDS # 72-0479] wolframite CoWO<sub>4</sub> monoclinic phase. The estimated lattice parameters of the CoWO<sub>4</sub> nanostructures are  $a = 4.949 \text{ \AA}$ ,  $b = 5.680 \text{ \AA}$ ,  $c = 4.696 \text{ \AA}$  and  $\beta = 90.0^\circ$ . These values have very good agreement with the previous reports [4, 9, 10]. However, in our study no Yb<sub>2</sub>WO<sub>6</sub> phase was observed even at 600 °C calcinations as reported by Naik et al. [8]. With respect to the Yb doping concentration, there is no peak shift was observed but the intensity decreased gradually. This implies the addition of Yb<sup>3+</sup> ion in the Co<sup>2+</sup> site reduces the crystalline size of the CoWO<sub>4</sub>. The mean particle diameter of the pure and doped CoWO<sub>4</sub> nanocrystals was estimated from the Scherer Equation [11].

$$d = k\lambda/\beta\cos\theta \quad (1)$$

where  $\beta$  is the full width half-maximum value of the high intensity peak,  $k$  is the so-called shape factor, and  $\lambda$  is the wavelength of the X-ray source used in the XRD. The obtained  $d$  values are about in the range of 60–80 nm. These values are fairly agreed with the FESEM and TEM observation.

### 3.3 FTIR studies

Figure 3 shows the FTIR spectra of pristine and Yb<sup>3+</sup> doped CoWO<sub>4</sub> nanoparticles. In order to determine the chemical structure of the sample the FTIR spectra was observed over the frequency range of 400–4,000 cm<sup>-1</sup>.

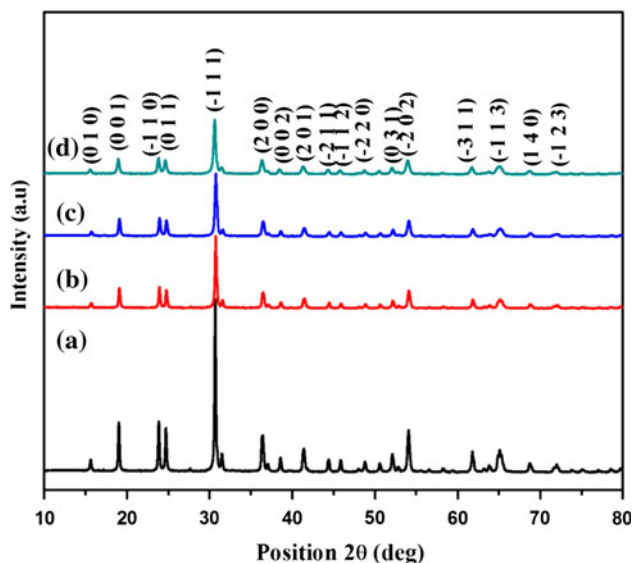


**Fig. 2** XRD pattern of wolframite pure (a) and different concentrations Yb doped CoWO<sub>4</sub> (b) 1 %, (c) 3 % and (d) 5 %

Intense band appeared in the low frequency region of 400–1,000 cm<sup>-1</sup> which belongs to the characteristic deformation modes of Co–O, W–O and W–O–W bridges. IR spectra below 500 cm<sup>-1</sup> could have been due to the deformation modes of W–O bonds in WO<sub>6</sub> octahedra or the deformation of W–O–W bridges [12]. The bands positioned at 820 and 621 cm<sup>-1</sup> were associated to the O–W–O vibration mode and the W–O bond stretching, respectively [13, 14]. The strong intense band in the region of 3,000–3,800 cm<sup>-1</sup> corresponds to OH stretching vibration of surface absorbed or internally bonded water molecules [15]. The bending mode of H–O–H is located at about 1,640 cm<sup>-1</sup>. The absorption of CO<sub>2</sub> from the atmosphere at the CoWO<sub>4</sub> surface was identified from the sharp peak positioned at about 2,370 cm<sup>-1</sup> in FTIR spectra. From the figure it can be seen that the intensity of O–C–O stretching band increases with increasing the concentration of Yb<sup>3+</sup>. This may be due to the presence of Yb<sup>3+</sup> in Co<sup>2+</sup> site that absorbs more CO<sub>2</sub> from air during calcinations.

### 3.4 Electron microscopy analysis

The HRSEM images of the pure CoWO<sub>4</sub> and the Yb doped compounds were taken at different magnifications are shown in Fig. 4a–h. The observed HRSEM images show the particles are in round edged cubical morphology with uniform distribution. All the samples are showing nearly the same morphological features with an average particle size of 40–60 nm. This infers that the addition of Yb does not affect the crystal structure which confirms the incorporation of Yb on to Co lattice site. While increasing the doping concentration the particle size was considerably reduced and aggregated. For further confirmation, TEM

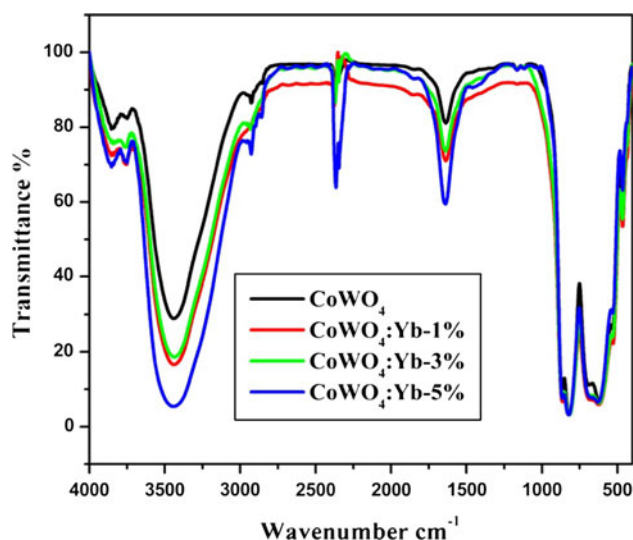


**Fig. 3** FTIR spectra of pure and Yb doped CoWO<sub>4</sub> heat treated at 600 °C

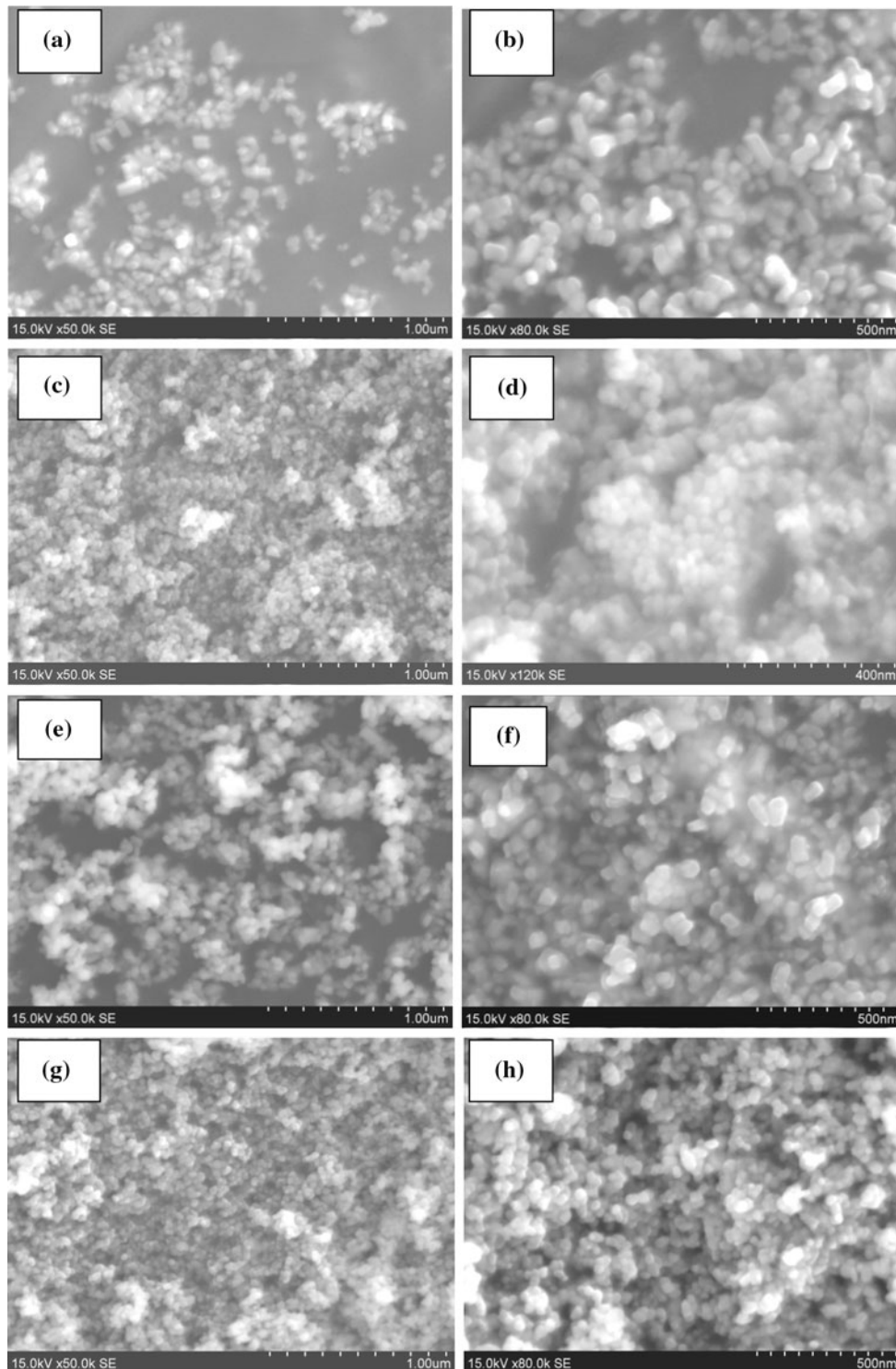


**Fig. 4** HRSEM images of pure (a, b), 1 %-Yb doped (c, d), 3 %-Yb doped (e, f) and 5 %-Yb doped (g, h)

observation was taken for pure and 3 % Yb doped  $\text{CoWO}_4$  with different magnification as shown in Fig. 5a–e. This image clearly gives evidence to the formation of round edged cubical  $\text{CoWO}_4$  nanoparticles. With the addition of Yb (3 %) it was observed that there is no change in

morphology. Even though, the measured intensity of the fringes in the SAED pattern as shown in Fig. 5f for the 3 % Yb doped  $\text{CoWO}_4$  concludes the particles are well crystalline and equally distributed. An increase in yttrium content leads to uniform and smaller particle size.



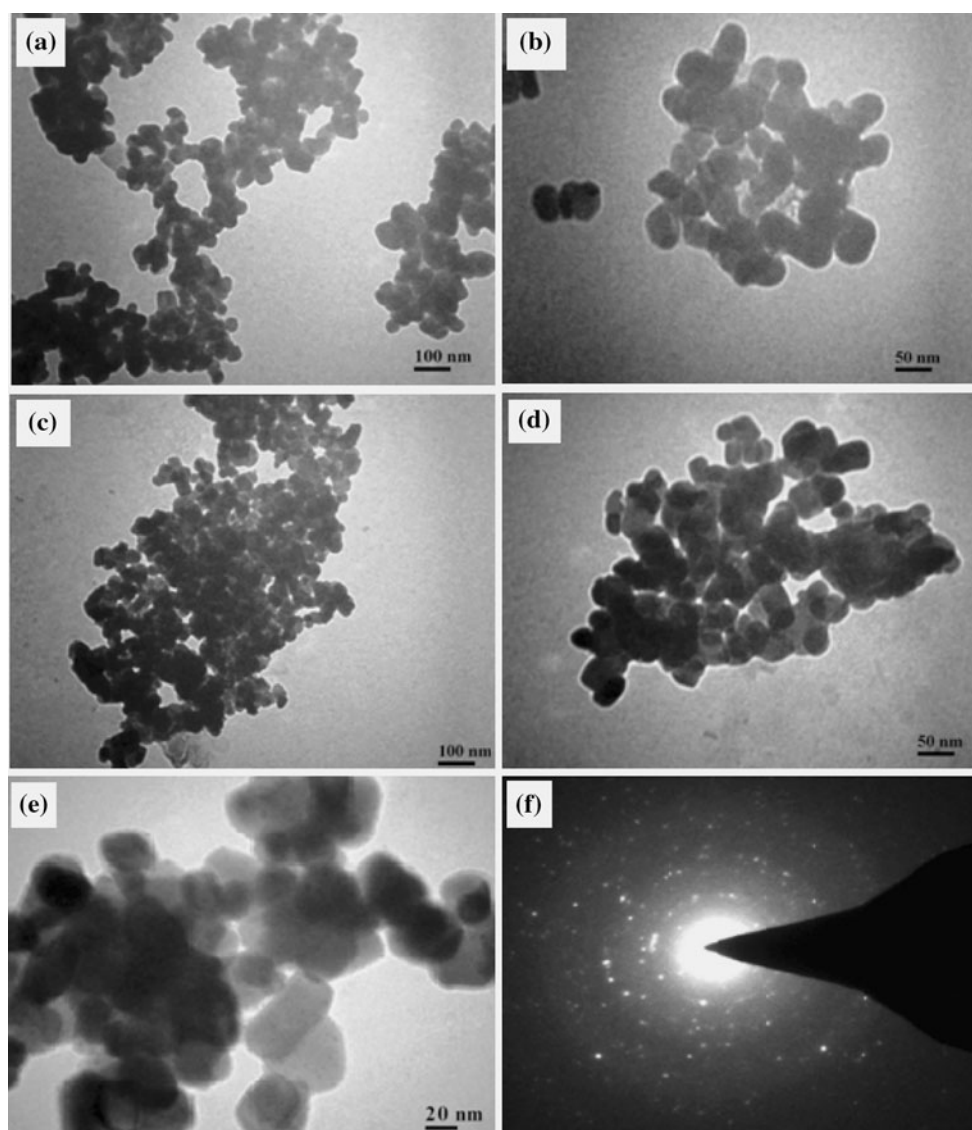


**Fig. 5** TEM metaphors of  $\text{CoWO}_4$  nanostructure for pure (a, b) and 3 % Yb doped (c–e) sample with different magnifications, (f) SAED pattern of 3 % Yb doped  $\text{CoWO}_4$

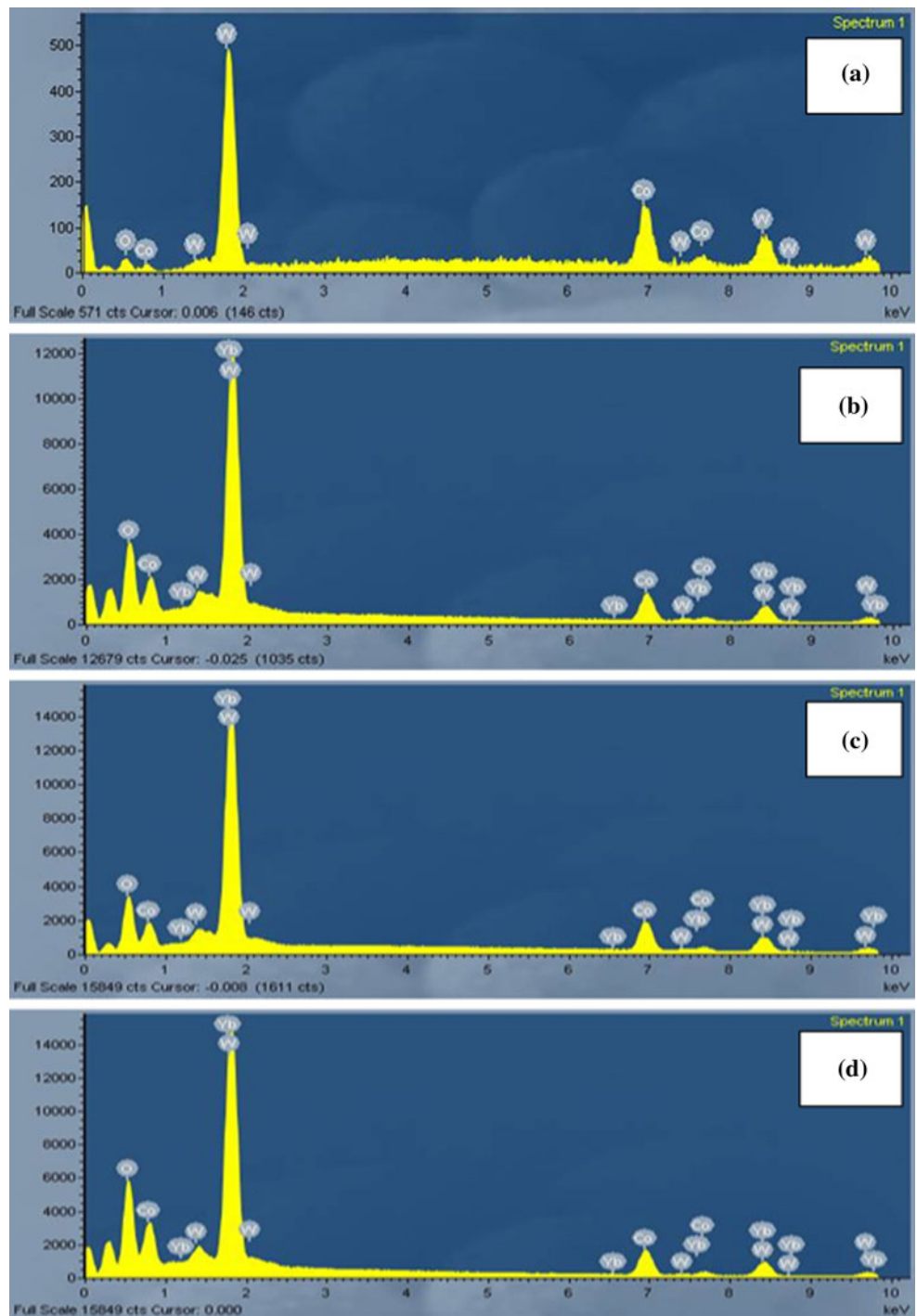
The compounds were found to have well distributed particles and polycrystalline in nature. The composition and the element present in the compounds were studied using EDS analysis which is illustrated in Fig. 6. This indicates that all the elements were present in the appropriate amount without any impurities. This describes the atomic scale stoichiometry of the compound.

### 3.5 UV–Visible spectral studies

Optical absorption spectra of pure wolframite and trivalent Yb doped  $\text{CoWO}_4$  nanoparticles heat treated at  $600^\circ\text{C}$  is illustrated in Fig. 7. All samples exhibits the strong absorption maximum at around 270–300 nm, confirms the strong UV absorption of the material. It implies that these

absorption bands arises mainly from the charge transfer between ligand and metal within the  $(\text{WO}_4^{2-})$  groups but which is not caused by  $\text{Yb}^{3+}$  ion [16]. This confirms that the addition of Yb does not change the host  $\text{CoWO}_4$  matrix. Further it suggests that this absorption may be directly related to the formation of  $[\text{WO}_6]^{6-}$  complex within the wolframite structure. In the excited  $(\text{WO}_4^{2-})$  state, the hole (on the oxygen) and the electron (on the tungsten) can form the excitons because of their strong interaction. In addition of Yb into  $\text{Co}^{2+}$  site it can be seen that there is peak shift towards lower wavelength with respect to the  $\text{Yb}^{3+}$  concentrations. This may be due to the active interaction of trivalent cation with divalent ion which is due to the quantum confinement effect [17]. The strong d–d transition band was observed in the visible region (i.e. 500–700 nm)

**Fig. 6** EDS spectra of pure (a) and Yb doped  $\text{CoWO}_4$  1 %-Yb (b) 3 %-Yb (c) and 5 %-Yb (d)



which also shifted slightly towards high frequency with respect doping concentration [9].

### 3.6 Photoluminescence studies

Room temperature luminescent spectra of pure and Yb doped  $\text{CoWO}_4$  nanostructures under the excitation of 230 and 240 nm are shown in Fig. 8a, b. From the observed spectra it can be seen clearly, the prepared samples exhibit

the broad blue-green emission band centred at 453 nm with shoulders which are directly related to the radiative transition within the  $[\text{WO}_4]^{2-}$  tetrahedral group. Generally, it is noted that the luminescent efficiency is strongly associated with the synthesizing process for obtaining particles with the shape of a non-agglomerate as well as high crystallinity [8, 9, 16, 18–20]. It is observed that the intensity of the spectra differs with respect to the doping concentration. In addition of Yb the luminescent intensity

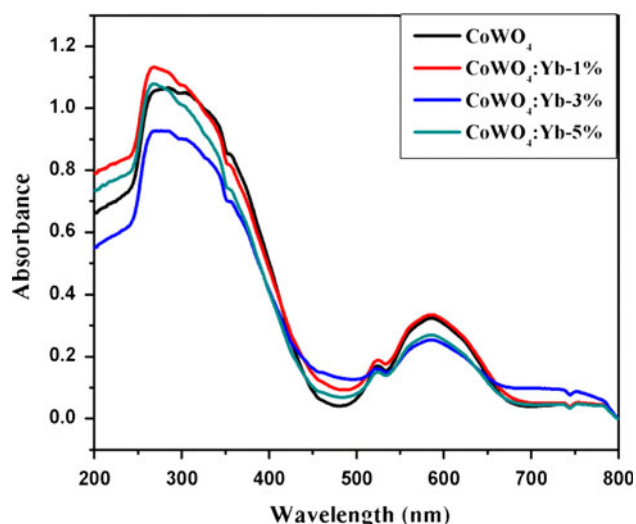


**Fig. 7** UV–Vis absorption spectra of  $\text{CoWO}_4$  nanostructure with various concentration of Yb

decreases up to 3 % then increases for high concentration. Naik et al. [8] reported the enhanced luminescent intensity in the  $\text{CoWO}_4$  due to  $\text{Ce}^{3+}$  doping up to 2 % and further addition it decreases significantly. In this study the addition of Yb suppresses the luminescent characteristic of the wolframite  $\text{CoWO}_4$  even at higher concentration. This is possibly due to the reduction of  $[\text{WO}_6]^{6-}$  phase formation in the  $\text{CoWO}_4$  nanostructure which reduces the annihilation process that results in the less intrinsic luminescence. Furthermore, with the addition of  $\text{Yb}^{3+}$ , crystallinity of the sample reduces considerably which also influencing the reduced luminescence behavior [20–22]. The enhanced luminescence intensity at the higher concentration 5 % may be attributed to the oxygen defect formation. This is confirmed by the presence of weak green emission band at 550 nm region [8, 20]. The positions of the emission peak in the PL spectra are the same for pure and  $\text{Yb}^{3+}$ -doped samples, this confirms the emission centre does not alter by the addition of Yb on to the  $\text{CoWO}_4$ . Though, there is no emission peaks appeared for Yb in the PL spectra, the characteristic PL intensity of the  $\text{CoWO}_4$  nanostructure found to reduce. This concludes that the addition of Yb in the  $\text{CoWO}_4$  could not enhance the luminescent behavior up to 5 %, in this continuation further investigation with the higher concentration will be the hope for optical enhancement in the wolframite structure.

### 3.7 Magnetization studies

Magnetic behavior of  $\text{CoWO}_4$  with the addition of  $\text{Yb}^{3+}$  was studied at room temperature. Yttrium is one of the rare earth ions which are most widely studied for optoelectronic devices. Magnetization of  $\text{Yb}^{3+}$  doped  $\text{CoWO}_4$ ,

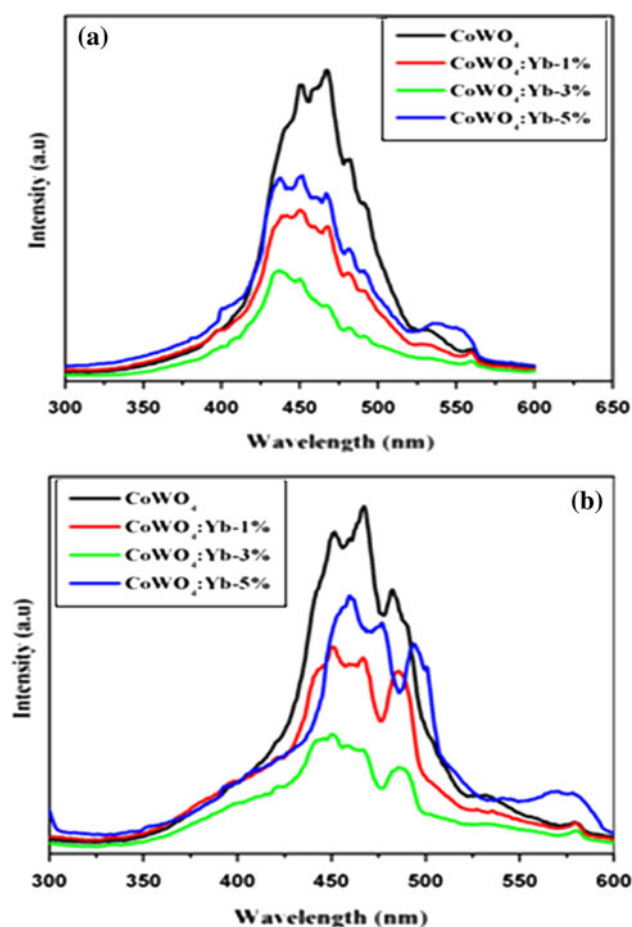


**Fig. 8** PL spectra of pure and Yb doped  $\text{CoWO}_4$  nanostructure excited at 230 nm (a) and 240 nm (b)

with respect to the applied magnetic field measured at room-temperature using VSM is shown in Fig. 9. All the samples show typical hysteresis loop, indicating a ferromagnetic ordering at room temperature. When compared to pure  $\text{CoWO}_4$ ,  $\text{Yb}^{3+}$  doped sample exhibits the enhanced ferromagnetic ordering with S-shape hysteresis curve at lower concentration [23]. With increase the doping concentration, the hysteresis loop move towards diamagnetism predominantly. This suggests the contribution of diamagnetism in high applied magnetic field. This may be due to the presence of  $\text{Yb}^{3+}$  ion in the Co site reduces the exchange coupling interaction within the ferromagnetic layer aligned antiferromagnetically within the tungstate [24]. The coercivity ( $H_c$ ) measured from the plot is 458.35, 464.21, 469.15 and 471.08 G for the pure and 1, 3 and 5 % Yb doped  $\text{CoWO}_4$  respectively. Generally, the metal tungstates exhibit paramagnetic behavior; in this case the origin of weak ferromagnetism was possibly due to the oxygen vacancies which can induce the exchange interaction between the spins of their unpaired electrons at the surface of the nanoparticles [25]. While doping with the rare earth element, ferromagnetic interaction either

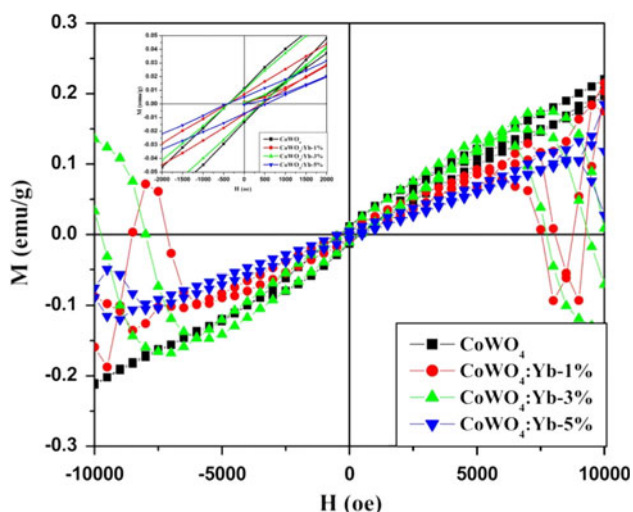


**Fig. 9** Hysteresis curve of pure and Yb doped  $\text{CoWO}_4$  nanostructure

suppressed or increased depending upon the rare earth magnetic ions. Basically, the magnetic properties are strongly associated to the magnetic ions and their interaction with the host material. Especially, the desired magnetic interaction response of the material is mainly by  $s$  electron for metal ions,  $p$ - $f$  electrons for rare earth magnetic ions [25]. Thus, further investigation is needed for the clear understanding of the typical magnetic behavior of the Yb doped  $\text{CoWO}_4$ .

#### 4 Conclusions

In this present investigation, we adopt the single step solution based chemical precipitation technique to synthesize the pure and Yb doped  $\text{CoWO}_4$  nanostructure. XRD pattern of the samples shows monoclinic phase with polycrystalline nature. The addition of Yb up to 5 % does not found any secondary phases due to the  $\text{Yb}_2\text{O}_3$ . From HRSEM and TEM observation round edged nanocubical surface morphology was confirmed. UV–Vis absorption analysis of  $\text{Yb}^{3+}$  doped  $\text{CoWO}_4$  exhibits the intense UV absorption at 278 nm which confirms the excellent optical behavior of the wolframite structure. The small shift towards high frequency region for the doped samples addressing the interaction of  $\text{Yb}^{3+}$  ion with  $\text{CoWO}_4$  structure. PL emission peak centered at 453 nm region shows the suppressed luminescence characteristics of the  $\text{CoWO}_4$  doped with  $\text{Yb}^{3+}$  ions. These studies conclude the choice of Yb ion for  $\text{CoWO}_4$  is not suitable for luminescent enhancement up to 5 %, we believe further increasing concentration of Yb will enhance the optical behavior of  $\text{CoWO}_4$  potentially. Alternatively, the typical synthesis process also would greatly influence the optical features of

the metal tungstates. Magnetization curve showed the presence of room temperature weak ferromagnetism of the  $\text{CoWO}_4$  disturbed considerably by the doped rare earth ion. Further, investigations on the magnetic behavior of the various rare earth magnetic ion doped wolframite structure will be the hopeful candidate for spintronics and optoelectronic devices applications.

**Acknowledgments** Authors greatly acknowledged to the Sophisticated Analytical Instrumentation Facility (SAIF), Indian Institute of Technology Madras (IITM), India, for provide the analytical instruments to carry out the analysis for our materials.

#### References

1. E. Tomaszewicz, *Thermochim. Acta* **447**, 69–74 (2006)
2. A. Sen, P. Pramink, *J. Eur. Ceram. Soc.* **21**, 745–750 (2001)
3. A. Phuruangrat, T. Thongtem, S. Thongtem, *Curr. Appl. Phys.* **10**, 342–345 (2010)
4. S. Rajagopal, D. Nataraj, O.Y. Khyzhun, Y. Djaoued, J. Robichaud, D. Mangalaraj, *J. Alloy. Compd.* **493**, 340–345 (2010)
5. Q. Dai, H. Song, X. Bai, G. Pan, S. Lu, T. Wang, X. Ren, H. Zhao, *J. Phys. Chem. C* **111**, 7586–7592 (2007)
6. S. Thongtem, S. Wannapop, T. Thongtem, *Ceram. Int.* **35**, 2087–2091 (2009)
7. Y. Huang, K.H. Jang, K. Jang, H.J. Seo, *J. Lumin.* **122–123**, 47–50 (2007)
8. S.J. Naik, U. Subramanian, R.B. Tangsali, A.V. Salker, *J. Phys. D Appl. Phys.* **44**, 115404 (2011)
9. S.J. Naik, A.V. Salker, *Solid State Sci.* **12**, 2065–2072 (2010)
10. L. Zhen, W.-S. Wang, C.-Y. Xu, W.-Z. Shao, L.-C. Qin, *Mater. Lett.* **62**, 1740–1742 (2008)
11. H. Emadi, M. Salavati-Niasari, F. Davar, *Polyhedron* **31**, 438–442 (2012)
12. F. Lei, B. Yan, *J. Am. Ceram. Soc.* **92**(6), 1262–1267 (2009)
13. F. Shi, J. Meng, Y. Ren, Q. Su, *J. Phys. Chem. Solids* **59**(1), 105–110 (1998)
14. J. Zhang, Y. Zhang, J.-Y. Yan, S.-K. Li, H.-S. Wang, F.-Z. Huang, Y.-H. Shen, A.-J. Xie, *J. Nanopart. Res.* **14**, 796–805 (2012)
15. Q. Zhang, W.-T. Yao, X. Chen, L. Zhu, Y. Fu, G. Zhang, L. Sheng, S.-H. Yu, *Cryst. Growth Des.* **7**(8), 1423–1431 (2007)
16. T. George, S. Joseph, A.T. Sunny, S. Mathew, *J. Nanopart. Res.* **10**, 567–575 (2008)
17. S.S. Ashtaputre, A. Nojima, S.K. Marathe, D. Matsumura, T. Ohta, R. Tiwari, G.K. Dey, S.K. Kulkarni, *J. Phys. D Appl. Phys.* **41**, 015301–015305 (2008)
18. Y. Wang, J. Ma, J. Tao, X. Zhu, J. Zhou, Z. Zhao, L. Xie, H. Tian, *Ceram. Int.* **33**, 1125–1128 (2007)
19. T. Thongtem, A. Phuruangrat, S. Thongtem, *Curr. Appl. Phys.* **8**, 189–197 (2008)
20. J.H. Ryu, J.-W. Yoon, K.B. Shim, *Solid State Commun.* **133**, 657–661 (2005)
21. G.Y. Hong, B.S. Jeon, Y.K. Yoo, J.S. Yoo, *J. Electrochem. Soc.* **148**(11), H161–H166 (2001)
22. S.H. Wu, H.C. Cheng, *J. Electrochem. Soc.* **151**(7), H159–H163 (2004)
23. K. Karthik, S. Kesava Pandian, K. Suresh Kumar, N. Victor Jaya, *Appl. Surf. Sci.* **256**, 4757–4760 (2010)
24. C.P. Landee, E.F. Westrum Jr., *J. Chem. Thermodyn.* **8**, 471–491 (1976)
25. R. John, R. Rajakumari, *Nano Micro Lett.* **4**(2), 65–72 (2012)